THE JOURNAL OF PHYSICAL CHEMISTRY C

ARTICLE

pubs.acs.org/JPCC

Chiral Domains Achieved by Surface Adsorption of Achiral Nickel Tetraphenyl- or Octaethylporphyrin on Smooth and Locally Kinked Au(111)

Lieve G. Teugels, L. Gaby Avila-Bront, and S. J. Sibener*

The James Franck Institute and Department of Chemistry, The University of Chicago, 929 East 57th Street, Chicago, Illinois 60637, United States

ABSTRACT: The self-assembly of either nickel tetraphenylporphyrin (NiTPP) or nickel octaethylporphyrin (NiOEP) on a reconstructed Au(111) surface is studied using scanning tunneling microscopy in ultrahigh vacuum. Even though the porphyrins are achiral in the gas phase, they are shown to form racemic chiral domains on the surface. For NiTPP we observe the expected roughly "square" unit cell as well as a new "parallelogram" unit cell. For NiOEP we find a hexagonally packed structure in which alternating rows are rotated 15° with respect to each other. We discuss the forces responsible for the formation of chiral domains and find intermolecular interactions to be the dominant factor in the assembly when the porphyrins are on a flat surface. Moreover, we observe that it is possible to break the formation of racemic domains of NiTPP on Au(111) by using a kinked vicinal surface as a symmetry-breaking template to locally lift the structural equivalence of the racemic surface structures. This study shows that a delicate interplay of intermolecular forces and adsorbate−surface interactions leads to the formation of complex structures and chiral phenomena.

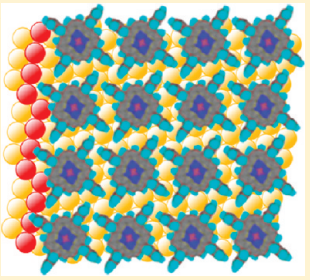

INTRODUCTION

The self-assembly of organic molecules on metal and semiconductor surfaces provides a promising route in the bottom-up fabrication process of nanostructures. Metalloporphyrins have been found to self-assemble into a variety of structures on a substrate, depending on the surface,[1,2] the surface temperature,[3] and the functional groups of the porphyrin ligands.[4,5] The exact structure is controlled by a delicate balance between intermolecular noncovalent binding forces and molecule−substrate interactions. Metalloporphyrins play an important role in biological processes such as photosynthesis (through chlorophyll) and oxygen transport (through hemoglobin). This has inspired their use in various technological applications. Examples include functionalized porphyrins being used as photosensitive dyes in photovoltaic cells[6−8] and as receptors in chemical gas sensors.[9] They have also been shown to have promising nonlinear optical,[10,11] spintronics,[12] and catalytic[13−16] properties. The virtually limitless porphyrin functionalization possibilities with different central metal atoms and ligands allows for the design of surfaces with physical and chemical properties tailored to the application's specific needs.[17] Self-assembled arrays of metalloporphyrins are especially practical because the correct combination of substituent groups and molecule−substrate interactions makes it possible for the arrays to form at room temperature and remain stable over a useful temperature range, making their incorporation into technological applications feasible. Adlayer structures of metalloporphyrins have been studied both in ultrahigh vacuum (UHV) and in solution by a variety of techniques, most prominently scanning tunneling microscopy (STM).

An interesting aspect of self-assembled arrays is the possibility to make chiral domains of adsorbates. Ever since Pasteur first uncovered the direct correlation between the structure of a crystal and the handedness of its component molecules,[18] researchers have been intrigued by the mechanism of chiral separation.[19,20] Chirally resolved surfaces provide a realistic approach for the separation of enantiomers.[21] Most commonly, chirally resolved surfaces are prepared by the adsorption of a self-assembled layer of chiral or achiral molecules.[22] Chiral adsorbates will spontaneously separate into left and right handed domains to pack into the most energetically favorable conformation.[23−25] Achiral adsorbates can also form organizationally chiral domains due to local intermolecular interactions and the symmetry breaking properties of surfaces. The adsorption of achiral molecules onto a surface can cause the formation of chiral domains as well, one of the earliest examples being the self-assembled chiral arrays formed by benzene on several different surfaces.[24] The structure of such an adlayer and the resolution of its enantiomeric domains is the result of a delicate balance of lateral molecule−molecule interactions and adsorbate−substrate forces.[26]

When chiral domains form on a surface, by the adsorption of chiral or achiral molecules, it is expected that equal numbers of left- and right-handed domains will form (a racemate).[27] It has been shown that chirality can be induced in achiral systems by introducing a new chiral entity, such as a high index crystal face[22] or a magnetic field.[28] Single enantiomer domains have shown promise in a number of fields, including asymmetric catalysis.[21,29]

Received: November 12, 2010
Revised: December 31, 2010
Published: January 27, 2011

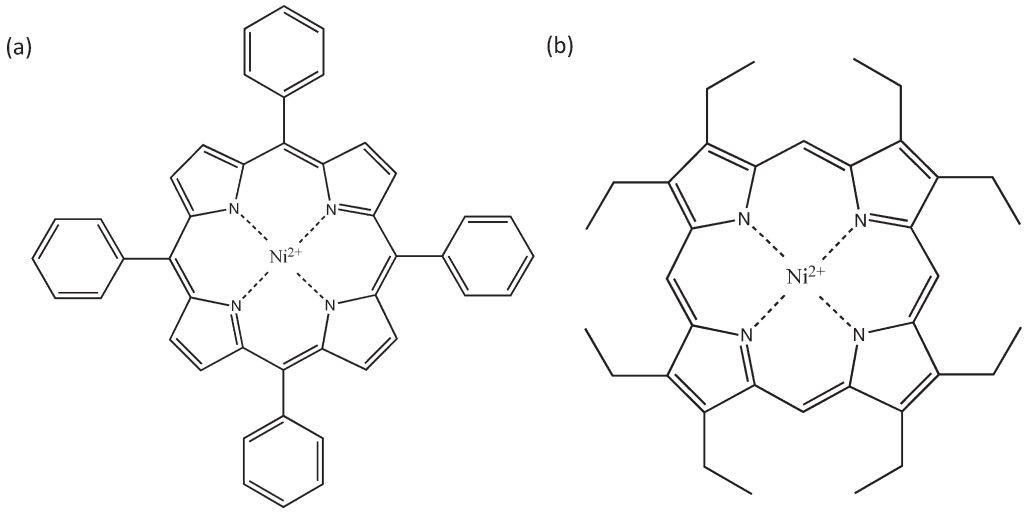

Figure 1. The structures of both porphyrin molecules that were used in this study: (a) nickel 5,10,15,20-tetraphenyl-21H,23H-porphine (NiTPP) and (b) nickel 2,3,7,8,12,13,17,18-octaethyl-21H,23H-porphine (NiOEP).

The exact chiral structure of such domains is governed by a variety of interactions.[30,31] First, molecules can form chiral domains by being constrained to two dimensions on a surface. Whether or not chiral arrays form usually depends on which face of the molecule adsorbs parallel to the substrate. Second, the substrate lattice plays an important role as it can guide self-assembled arrays to align with the main lattice directions, which can lead to the formation of a chiral array. The substrate can induce chirality within the molecule itself as well by forcing the molecule to rearrange its internal structure to accommodate substrate−adsorbate interactions.

Intrinsically chiral crystal lattices are also used to induce of chiral discrimination. It has been shown that a bulk crystal lattice with a high Miller Index is chiral if its steps are kinked.[32] The kinks expose microfacets of intersecting surface planes whose rotational progression is right- or left-handed. However, the chirality of a crystal surface is not limited to a bulk crystal with a high Miller index. Achiral crystals can also be locally chiral as a result of a miscut or defect. In the surface used in this study, for example, defects in the form of kinked steps were purposely sought out to study areas of local chirality. The ability of a surface to guide self-assembly and act as a template for adsorbates presents a pathway for the creation of nanoscale systems that can be applied to industrial processes leading to enantiospecific reactions or the production of optically active materials.[21]

Finally, we consider the role that intermolecular forces play in the formation of chiral arrays. Local interactions between individual molecules such as steric repulsion/attraction and hydrogen bonding can determine the structure of a self-assembled array. Whether or not the resulting structure is chiral depends on the relative extent of the forces and, for certain cases, on how closely the molecules are packed. In most cases, the chirality of an array is caused by a combination of all the interactions mentioned.

In this work we study the chirality of self-assembled arrays formed by the adsorption of vapor-deposited achiral nickel 5,10,15,20-tetraphenyl-21H,23H-porphine (NiTPP) or nickel 2,3,7,8,12,13,17,18-octaethyl-21H,23H-porphine (NiOEP) on a reconstructed 23 x $\sqrt{3}$ Au(111) surface using STM in UHV.[29−42] Their molecular structures are shown in Figure 1. It has been shown that this Au(111) surface enables the formation of ordered arrays, making it the ideal substrate for our studies.[43,44] Specifically, we look at how intermolecular forces and interactions with the substrate influence the formation of chiral domains. We report a new self-assembled structure for NiTPP consisting of a parallelogram-shaped unit cell as well as a square-packed arrangement. For NiOEP we find a roughly hexagonally packed structure with alternating rows rotated by 15°. In recent years, the structure of metal tetraphenyl- and octaethylporphyrin adlayers has received much interest, although no comments have been made on the chirality of the adlayer domains. Tetraphenylporphyrin layers studied were found to form a well-organized overlayer with a roughly square unit cell on Au(111), both in solution and in UHV.[15,33−35] A roughly hexagonal unit cell was found for metal octaethylporphyrins on the same gold surface.[1,16,36−39] Literature results for either porphyrin show only one enantiomeric domain, even though both mirror image domains exist, as we show in this work. Previous studies on tetraphenyl- and octaethylporphyrin arrays also do not seem to comment on the emergence of chirality, a topic that we address in this work as well.

EXPERIMENTAL SECTION

All experiments were performed in a UHV chamber with a base pressure of 5×10^{-11} Torr using an Omicron micro-STM.[45] The Au(111) single crystal surface was prepared in UHV using several repeated sputtering (1 keV, Ne^+) and annealing (700−800 °C) cycles. Surface cleanliness was verified with Auger electron spectroscopy, and the surface order was ascertained by low-energy electron diffraction. STM imaging confirmed the quality of the surface and the presence of the herringbone reconstruction. NiTPPs and NiOEPs were purchased from Sigma Aldrich and used without further purification. The porphyrins were deposited onto a room temperature Au(111) surface from a Knudsen-cell type setup consisting of a quartz crucible wrapped with a heating filament. Optimal evaporation parameters for monolayer and submonolayer porphyrin coverage were determined through a series of experiments where we varied crucible temperature and dosing time. We combined AES data and STM images to determine the quality of the deposited adlayer. STM imaging was performed using electrochemically etched Pt/Ir tips at room temperature in constant current mode and then filtered and slightly smoothed.[46] Scanning tunneling

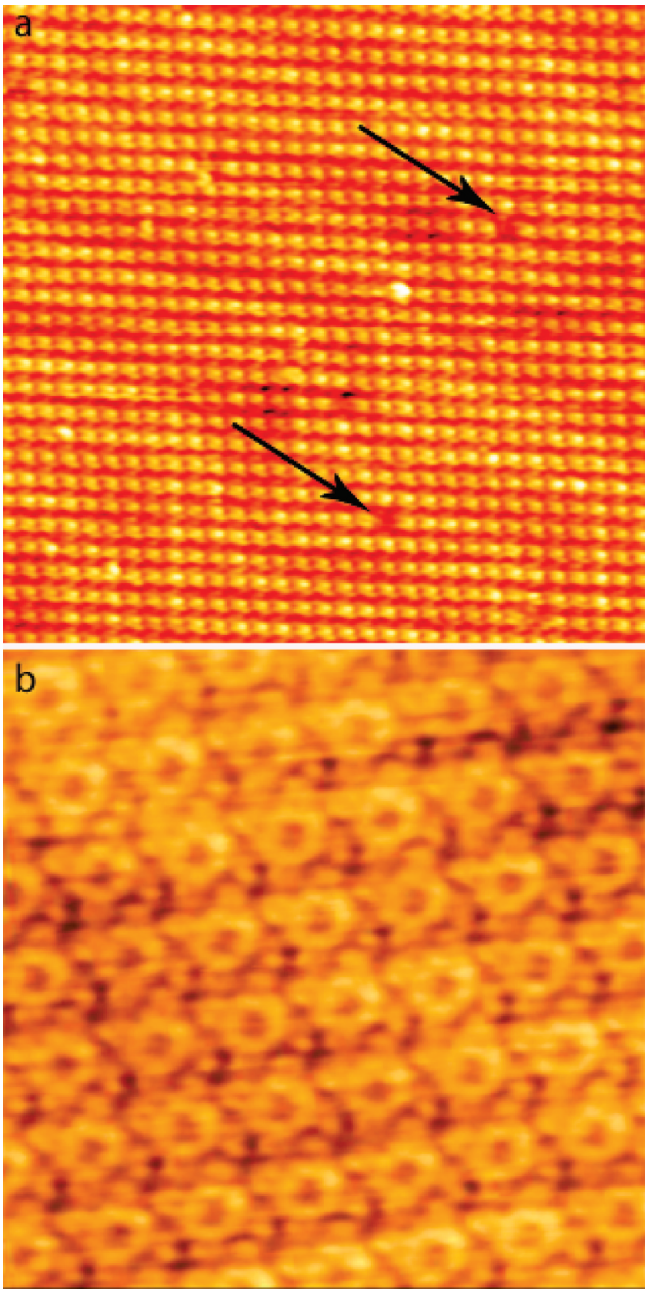

Figure 2. (a) STM image of a vapor-deposited NiTPP monolayer on a Au(111) substrate, acquired at 1.0 nA and 0.5 V (41 × 41 nm^2). Arrows indicate possible vacancies or nonmetalated porphyrins. The gold herringbone reconstruction is clearly visible underneath the porphyrin overlayer. (b) Zoomed-in STM image of the S′ domain acquired from a different sample than that used to produce Figure 1a. Imaging parameters are 2.0 nA and 1.0 V, 8.6 × 8.6 nm^2. In this image, the interdigitation of the phenyl substituent groups is clearly shown.

spectroscopy (STS) data were obtained by taking I/V spectra of the adlayer, converting them to dI/dV curves, averaging the results over 15−20 spectra and then smoothing them.

RESULTS AND DISCUSSION

a. NiTPP on Au(111). Figure 2a shows a typical large-scale STM image of a NiTPP monolayer on Au(111). The NiTPP molecule is converted from the D_{4h} symmetry it had in the gas

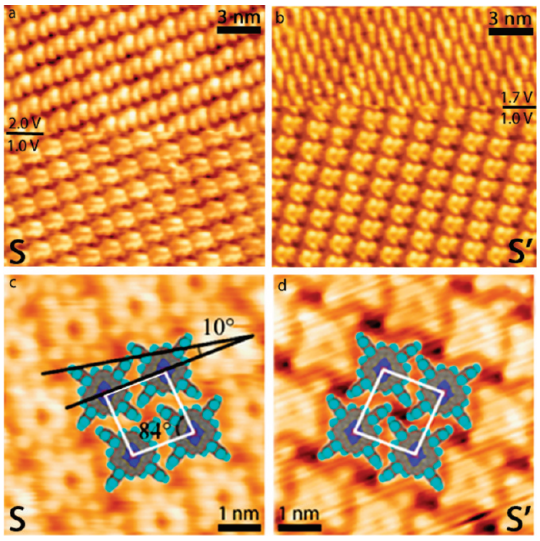

Figure 3. STM image of (a) S and (b) S′ domains acquired at 1 nA with a bias change (indicated by white line) from 2.0 to 1.0 V and from 1.7 to 1.0 V, respectively. (c,d) A detailed STM image of NiTPP domains showing the S and S′ enantiomer conformations, acquired at 1.0 nA, 1.5 V and 1.0 nA, 1.0 V, respectively. Overlaid is a three-dimensional (3D) structural model and the unit cell is marked. Each unit cell measures 1.36 ± 0.04 nm by 1.46 ± 0.04 nm with an acute angle of 84° ± 3° and contains one NiTPP molecule. The 10° rotation of the porphyrins with respect to their main unit cell direction makes chiral domains possible.

phase to D_{2d} symmetry when adsorbed onto the surface. The evaporated NiTPP molecules form large, well-organized domains on the gold surface and the porphyrin overlayer does not inhibit our observation of the gold herringbone reconstruction beneath the adlayer. We observed what appear to be vacancies in the NiTPP overlayer but the overall number measured below 1%. These vacancies could be either missing porphyrin molecules or nonmetalated H_2TPP molecules.[47] Figure 2b shows a zoomed-in STM image of a NiTPP monolayer from a different sample. In this image, the interdigitation of the phenyl rings is clearly resolved. An extensive examination of the STM images of the NiTPP arrays revealed the existence of two distinct conformations: a roughly square or rhomboid (S) structure (which we will simply call "square" from now on) and a parallelogram (P) structure. In addition, for each conformation, we observed domains of their rotational mirror image S′ and P′. Our data indicates that a racemic structure formed on the surface, as one would expect. STM images of the two mirror image S and S′ structures are shown in Figure 3c,d with a molecular model overlay. The square conformation is comparable to most of the conformations reported for assemblies of metal tetraphenylporphyrins on Au(111) in literature, although the existence of mirror image domains was never reported for tetraphenyl porphyrins with a nickel central metal on one sample of Au(111). To the best of our knowledge, the parallelogram structure has not previously been reported.

At lower resolution, individual NiTPP molecules appear as rounded square features with a depression in the center. The nickel atom appears as a depression because of the lower tunneling probability of the filled nickel d_z^2 orbital.[48,49] At higher resolution, the four phenyl groups can be distinguished at the corners while the internal structure of the porphyrin ring becomes clearer. Some images show the pyrrole rings as a double

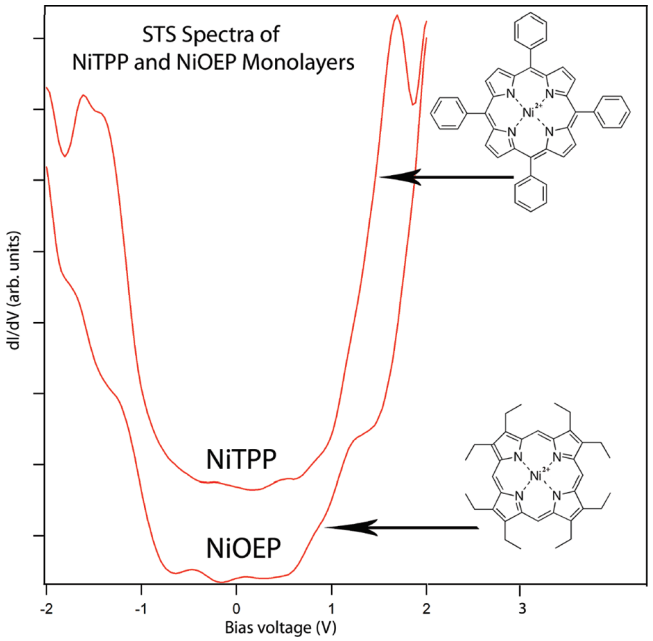

Figure 4. STS spectrum of a NiTPP and a NiOEP adlayer on Au(111) acquired at 1.5 V and 0.4 nA.

protrusion on two opposite sides, as shown in Figure 3d. This indicates that the porphyrin is slightly deformed to a saddle shape, as noted by Auwärter et al.[50,51] The Auwärter study suggested that the terminal phenyl groups are alternately rotated out of the porphyrin plane. Steric repulsion between the hydrogen atoms on the porphyrin ring and the phenyl groups causes one pyrrole pair to tilt upward. This tilting, combined with the 2-fold symmetry of the lowest unoccupied molecular orbital (LUMO)[52,53] causes the NiTPP molecule to appear as a two-lobed structure at imaging parameters with voltages around 1.5 to 2.0 V. This is clearly illustrated in Figure 3a,b, which shows STM images for both S and S′ structures where the bias voltage is changed from 2.0 or 1.7 to 1.0 V during the image. Figure 4 shows an STS spectrum of the NiTPP adlayer. The locations of the highest occupied molecular orbital (HOMO) peak at −1.3 to −1.4 V and the LUMO peak at 1.6−1.7 V are comparable to results published for NiTPP in literature.[33,54] The LUMO peak corresponds well with the bias voltage at which a noticeable change is observed in the STM images. At bias voltages above 1.5 V, the image changes from a molecule with 4-fold symmetry to a molecule with 2-fold symmetry, indicating resonance with the LUMO orbital of the system. This transition occurs for both the square and the parallelogram arrangements. Figure 5 shows a close-up STM image of the P and P′ conformations. Note that for simplicity and clarity, we used a molecular model overlay with the phenyl groups perpendicular to the surface. As mentioned earlier, in reality, when the NiTPP molecule adsorbs onto the surface, the NiTPP molecule takes on a saddle shape with a dihedral angle between the porphyrin plane and the phenyl group estimated to be between 60° and 90°.[2,55−57]

A detailed statistical analysis was performed on the STM images of the NiTPP monolayer. The analysis gave a unit cell of 1.36 ± 0.04 nm by 1.46 ± 0.04 nm with an acute angle of 84° ± 3° for the "roughly square" structure. The packing density is 5.0×10^{13} molecules/cm^2 and the apparent height is approximately 0.5 nm. Literature values for NiTPP specifically and metal

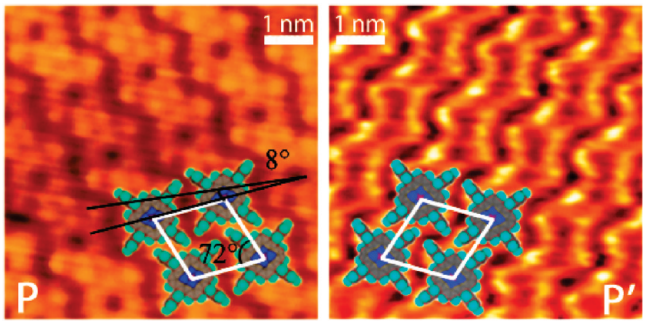

Figure 5. STM image of NiTPP domains on Au(111) showing the new P and P′ enantiomer conformations, acquired at 2.0 nA and 1.0 V for the P structure and 1.0 nA and 2.0 V for P′. Overlaid is a 3D structural model, and the unit cell is marked. Each unit cell contains one NiTPP molecule and measures 1.47 ± 0.07 nm by 1.56 ± 0.07 nm with an acute angle of 72° ± 3°. The 8° rotation of the porphyrins with respect to their main unit cell direction causes the emergence of chiral domains.

tetraphenylporphyrins in general[15,58,59] on Au(111) give unit cell dimensions of 1.40−1.43 nm and an angle of 85°, which correspond rather well with our findings. Individual enantiomer structures similar to S and S′ have been reported for NiTPP[34,60] on Au(111) and for H_2TPP[61,62] on Ag(111). For the parallelogram structure, a unit cell of 1.47 ± 0.07 nm by 1.56 ± 0.07 nm with an acute angle of 72° ± 3° is found with a packing density of 4.5×10^{13} mol/cm^2. Because of the pronounced difference in unit cell, it is possible to distinguish the two structures, even in lower resolution images. For both square and parallelogram conformations, the molecules are rotated 8−10° with respect to the main unit cell direction.[63] This slight rotation is crucial to making the formation of chiral domains possible. A thorough examination of numerous domains on several different samples shows that most of the domains have the square conformation, while only 5−10% show the parallelogram structure.

The small percentage for the parallelogram conformation could explain its absence in previous literature. It is a higher energy form because in the parallelogram structure the phenyl rings are closer to perpendicular with respect to the porphyrin plane, allowing $\pi-\pi$ interactions between phenyl rings of neighboring molecules.[64] The porphyrin ring is further away from the gold surface in the parallelogram conformation, which reduces the interaction with the gold and causes the energy of the arrangement to be higher. The square structure on the other hand does not have the possibility of $\pi-\pi$ interactions but is stabilized by interdigitation and T-type interactions between the hydrogen atom of a substituent phenyl group and the center of an adjacent phenyl group.[65] The more rhomboid unit cell dimensions for the "square" structure may be caused by interactions of the molecules with the gold surface underneath combined with the reduction of the internal symmetry of the molecule from 4-fold to 2-fold symmetry upon adsorption.

The precise location of the gold substrate in relation to the NiTPP monolayers could not be determined from our images. However, it is possible to estimate the position of the substrate from the herringbone reconstruction, which is imaged simultaneously with the NiTPP monolayers. On the basis of the structure of the herringbone, it is seen that NiTPP molecules are aligned with the underlying gold surface but are not commensurate with the gold lattice. A detailed study of NiTPP domain boundaries shows that different domains always intersect

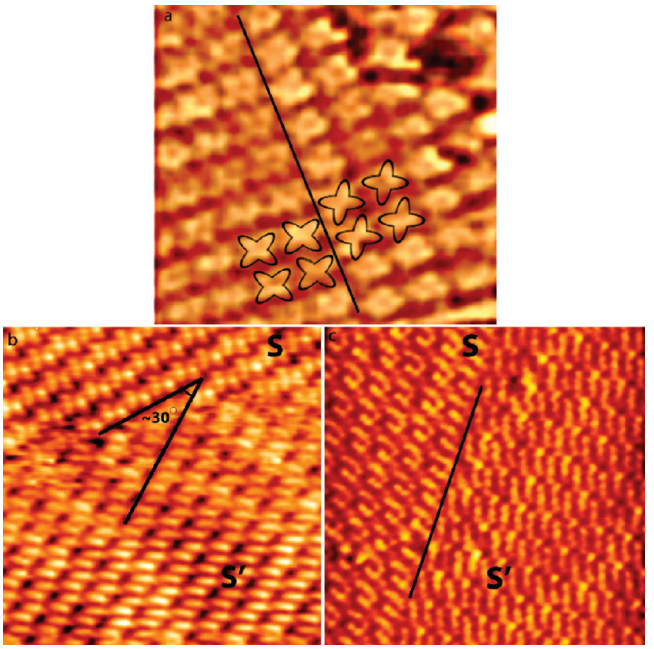

Figure 6. STM images of boundaries between NiTPP S and S′ domains, showing intersections. Domains only meet at angles of 0°, 30° or 60°, because the porporphyrin unit cell aligns with either one of the main directions of the gold or with the directions of the herringbone. Panels a−c clearly demonstrate that the S and S′ domains exist together in a single area. The translational shift between domains is shown in panel a. This longitudinal shift allows the molecules to maintain a T-type interaction between the phenyl groups. (a) The domain boundary occurs at 0°. Imaging parameters are 3.0 nA and 1.0 V, 80 × 80 nm^2. (b) The domain boundary occurs at 30°. Imaging parameters are 1.0 nA and 2.0 V, 16.7 × 16.7 nm^2. (c) The domain boundary occurs at 0°. Imaging parameters are 0.3 nA and 2.5 V, 15.5 × 15.5 nm^2.

at either 0°, 30° or 60° (±5°) angles.[66] Figure 6 shows two examples of these domain boundaries.

A review of STM images of metal tetraphenylporphyrin domain boundaries on Au(111) published in the literature confirms these angles. Because in most images the gold herringbone can be imaged through the NiTPP overlayer, we can conclude that there is a preference for the NiTPP domains to either follow one of the three herringbone or one of the three main gold directions. This would explain why the domain boundary angles are limited to roughly 0°, 30°, and 60°.

The domain boundaries shown in Figure 6 highlight the fact that both enantiomeric domains exist together on the same surface. This figure also clearly depicts how the molecules arrange themselves at domain boundaries. In Figure 6a, we observe a translational shift between the molecules on either side of the domain boundary as highlighted by the black line. With such a shift, the molecules are still able to arrange themselves with a T-type interaction.

The surface-induced directionality is exceptionally illustrated in Figure 7, where it is seen that NiTPP domains and adjacent kinked steps follow the same direction. The local kinked step is a chiral entity and nucleates the formation of only S′ domains. Thus, we see that the porphyrin array locally follows the handedness of the step. The NiTPP molecules adsorbed on the step edge appear to be bridging the step, with two phenyl groups interacting with the top and two phenyl groups interacting with the lower step. This behavior is similar to the adsorption

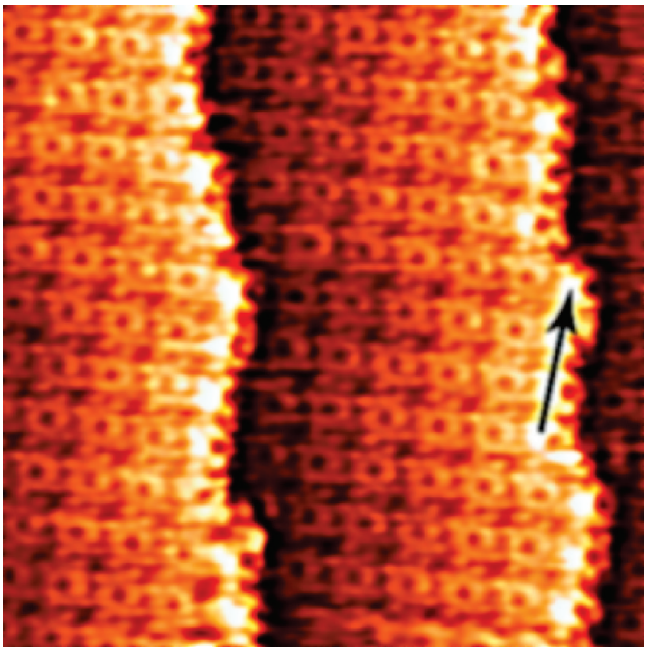

Figure 7. STM image of a NiTPP adlayer on three adjacent gold steps, acquired at 1.0 nA and 1.5 V (16.7 × 16.7 nm^2), showing the directionality of the porphyrin adlayer. This image suggests that kinks in the gold steps act as nucleation sites for domains of one particular enantiomer. The locally chiral surface with an estimated (336 316 315) surface plane guides the porphyrin molecules into single-handed domains. Molecules that sit on the step edge appear to bridge the step.

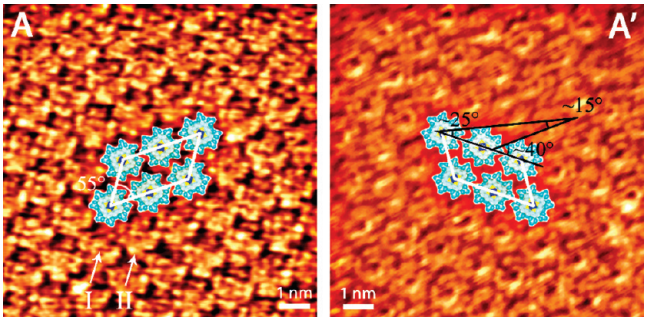

Figure 8. STM images of NiOEP domains showing the two enantiomer conformations, acquired at 0.5 nA and 3.0 V for structure A and 0.4 nA and 1.0 V for A′. Overlaid is a 3D structural model and the unit cell is marked. Each unit cell contains two porphyrin molecules and measures 2.86 ± 0.07 by 1.67 ± 0.11 nm with an acute angle of 55° ± 5°. Alternating rows are oriented differently (marked I and II) since they are rotated 15° with respect to each other. A 25° or 40° rotation with respect to the main unit cell causes the domains to be chiral.

of CoPc on stepped Au(788).[67] The height difference of approximately 0.25 nm confirms that the features are indeed gold steps and not a second porphyrin layer.

b. Nickel Octaethylporphyrin on Au(111). In order to gain more insight into the chiral self-assembly mechanism, we studied the adsorption of NiOEP on the Au(111) surface as well. In low-resolution STM images, NiOEP molecules appear as rounded square features with a central depression for the nickel atom, just like the NiTPP molecules. However, at higher resolution, the eight ethyl groups can be resolved as bright spots lining the porphyrin ring in the STM images, as shown

in Figure 8. The molecular overlay shows the mirror image A and A′ structures.

NiOEP forms a roughly hexagonally packed structure with molecules in neighboring rows twisted 15° with respect to each other. All molecules within each row indicated by arrows in Figure 8 are oriented the same way. However, two different orientations (denoted as I and II) exist, causing every second row to exhibit the same molecular orientation. Every NiOEP molecule also exhibits a slight rotation with respect to the main unit cell direction, which causes an overall chiral arrangement. The rotation is ∼40° for rows I and ∼25° for rows II, as shown in Figure 8. This structure corresponds with other reports for OEP arrays on Au(111), although the mirror image structures were never reported for the same molecule on one sample. Structure A was reported for NiOEP[36] and A′ for CoOEP,[14] but to the best of our knowledge the A′ structure was never reported for NiOEP on Au(111). Because NiOEP is harder to image than NiTPP, we were unable to collect as many images of the NiOEP assembly. Nevertheless, from our images, it was possible to estimate that the enantiomers occur in roughly racemic amounts. We determined the unit cell of the structure to be 2.86 ± 0.07 by 1.67 ± 0.11 nm with an acute angle of 55° ± 5°. Each unit cell contains two octaethylporphyrin molecules, leading to an overall packing density of 5.1×10^{13} molecules/cm^2. Hence, just like NiTPP, NiOEP molecules are achiral in the gas phase but form chiral domains on a substrate that are incommensurate with respect to the reconstructed gold surface underneath. This incommensurability is due to the size difference between the porphyrin superlattice and the gold lattice.

The adsorption onto the gold substrate causes the ethyl groups of the NiOEP molecule to point upward, forming a "bowl-like" shape.[36] This causes a reduction from D_{4h} symmetry in the gas phase to C_{2v} on the surface. Due to the upward rotation of the ethyl groups, the porphyrin ring can sit closer to the gold surface, allowing for a greater interaction with the gold. This causes the adsorption energy of NiOEP on Au(111) to be greater than that for NiTPP. Figure 4 contains an STS spectrum of the NiOEP adlayer, showing a shoulder for the HOMO peak around −1.2 to −1.3 V and a LUMO peak around 1.3 V.

c.1. Chiral Domains. Our discussion begins by addressing the adsorption of NiTPP on Au(111) and the formation of a racemic mixture of chirally resolved domains. The discussion continues by addressing how the structural symmetry responsible for racemic adsorption can be broken using kinked steps. We end our discussion by addressing how the porphyrins can restructure the gold herringbone reconstruction.

What drives the formation of chiral domains of these nickel porphyrins on Au(111)? We could not find isolated NiTPP or NiOEP molecules on the gold substrate to determine whether a single molecule undergoes the respective 8° to 10° or 15° rotation we observed, because the porphyrins are too mobile at room temperature. However, previous studies at cold temperatures and calculations indicate[55,68] that similar porphyrin molecules do not undergo a rotation when adsorbed onto a Au(111) substrate. This indicates that the slight rotation of the porphyrin molecules is not caused by the adsorption site. The central metal atom also seems to have a negligible effect on the chiral domain formation for either porphyrin. We used vapor-deposited CoTPP to confirm that even with a different central metal, tetraphenylporphyrins will form the same chiral structure and found both the S and S′ versions of the square structure for CoTPP on Au(111). Previous studies show that CuTPP, CoTPP, or ZnTPP[13,34] adlayers form a similar square-like arrangement on Au(111).[44] The negligible influence of the central metal atom is confirmed for OEP as well because FeOEP and CoOEP[14,38] form hexagonal structures on Au(111), which are very similar to the NiOEP domains. As we discussed earlier, the adsorption site does not seem to cause the formation of chiral domains, but the surface as a whole can influence the directionality of the self-assembled arrangements. However, those long-range interactions do not cause the emergence of chiral domains either. This is confirmed by the observation that both FeTPP and H_2TPP form structures on a different substrate, Ag(111),[50,61] that look very much like the square arrangement that we observed for NiTPP on Au(111). The influence of the substrate is illustrated for OEP by the fact that CuOEP forms a hexagonally packed structure without the slight rotation between rows when adsorbed onto NaCl layers on Ag(001).[69] NiOEP forms both a hexagonal and a squarely packed structure on graphite.[1] However, the difference in structure in that case can also be caused by the deposition method because the NiOEP adlayer was deposited from a benzene solution. The rotation angle of the NiOEP molecules with respect to the main unit cell was not determined, so we cannot compare it to the 15° angle we observed on Au(111). The effect of deposition method is expected to be minimal for NiTPP based on observations from previous studies that show that CoTPP and CuTPP form S and S′ structures on Au(111) when deposited from a benzene solution. Our conclusion is that the precise chiral structure of the porphyrin adlayer is caused by intermolecular van der Waals forces and hydrogen bonding interactions between neighboring porphyrin molecules, combined with a directionality caused by the gold surface.

c.2. Intermolecular Forces Drive Chiral Domains on Flat Terraces. In order to understand why the studied porphyrins formed the chiral packing structures we observed, we compared our two-dimensional (2D) monolayer crystals with 3D crystals that were grown from solution. X-ray diffraction data show that NiTPP crystals will form a tetragonal or a triclinic crystal, depending on the kind of seed used to start the crystallization process. The tetragonal NiTPP crystal has four molecules per unit cell and has dimensions $a = b = 15.04$ Å and $c = 13.92$ Å.[56] The triclinic structure on the other hand has a unit cell that contains only one porphyrin molecule and shows parameters of $a = 6.44$ Å, $b = 10.42$ Å, $c = 12.41$ Å, $\alpha = 96.06°$, $\beta = 99.14°$, and $\gamma = 101.12°$.[70] In both crystal structures, the porphyrins are rotated in the plane of the macrocycle with respect to the main directions of the unit cell. This angle is approximately 30° for the tetragonal and 20° for the triclinic structure. In both cases, the phenyl groups are rotated with respect to the plane of the porphyrin ring approximately 72° for the tetragonal, and 61−63° for the triclinic structures.[57] These angles are similar to the predicted rotation of the phenyl groups upon adsorption of NiTPP molecules onto a Au(111) surface.[2,55] In the triclinic crystal, no two porphyrin rings are located within the same plane, making the formation of a similar structure on a flat substrate rather unlikely since the porphyrins adsorb with the porphyrin ring parallel to the surface. The tetragonal structure on the other hand is a viable structure to compare with our 2D monolayers. The X-ray data show that laterally adjacent porphyrins in a crystal are rotated with respect to each other. This 15° rotation is similar to the 8−10° rotation we observed in our STM images. The rotation is inherent to the tetraphenylporphyrin system and caused by the intermolecular forces between porphyrins. This observation reinforces our argument that intermolecular forces are the main cause for the

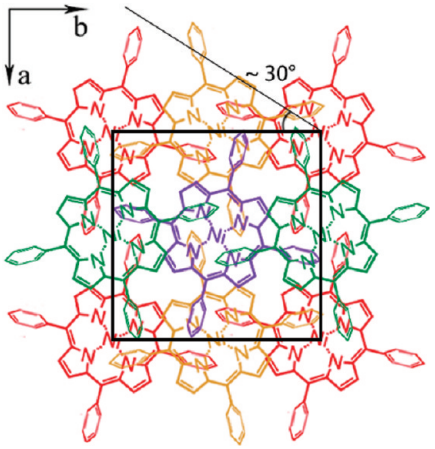

Figure 9. Model of the structure of a tetragonal NiTPP crystal, made using data from ref 53. The *a* and *b* directions of the unit cell are indicated, and the *c* direction is perpendicular to the plane of the paper. The molecules are color-coded red-brown-purple-green from the bottom layer to the top layer. The coordinates in the *c* direction are 0 (red), 1/4 (green), 1/2 (purple), and 3/4 (brown), showing that all layers are evenly spaced. The square base of the tetragonal unit cell is marked by the black square.

formation of chiral domains. The distance between the porphyrins is different for the crystal and the monolayer. In the crystal, neighboring porphyrins are ~15 Å apart, while we find 13.6 Å and 14.6 Å for the square and 14.6 Å and 15.7 Å for the parallelogram structure. The packing density in the crystal, 4.41×10^{13} molecules/cm^2, is markedly smaller than the square monolayer structure density (5.0×10^{13} molecules/cm^2) and slightly smaller than that of the parallelogram structure (4.65×10^{13} molecules/cm^2). The unit cell for the monolayer is also not rectangular. These differences are due to the significantly different surroundings in a crystal (several stacked porphyrin layers) versus a monolayer (vacuum and a gold substrate). In the monolayer, a closer approach allows interaction between the π-systems of the phenyl rings, stabilizing the structure. Besides the slight rotation and the twisted phenyl rings mentioned earlier, the crystal and the monolayer have another feature in common: in both cases the porphyrin has a saddle or "ruffled" shape. In the crystal the ruffling is caused by the presence of phenyl rings of the layer above interacting with the pyrrole rings of the porphyrin below, as can be seen in the structure shown in Figure 9. In a monolayer the ruffling is caused by an attraction of the porphyrin ring to the gold, combined with the twisted phenyl rings.[49,50] Although the interactions causing the configuration change are different, they show that ruffling is the preferred way for the porphyrin to respond to stress from its surroundings. Our main conclusion from the crystal−monolayer comparison is that the overall shape of the molecule is very similar in both setups. Also, the slight rotation that causes the organizational chirality in the monolayer is also present in the crystal, although the exact dimensions and angles of the unit cell are different. In the NiTPP crystal, left- and right-handed versions of the chiral structure occur in alternating layers, as can be seen in Figure 9, while in the monolayer they occur in segregated domains.

In the case of a NiOEP crystal, the comparison is harder, mainly because the porphyrin molecules in a crystal have a markedly different shape than in the monolayer. In our STM images, the NiOEP molecules showed a symmetrical distribution of bright spots in the location of the ethyl groups, indicating that they are pointing upward.[36] In a crystal, however, no matter whether it is triclinic or tetragonal, four ethyl groups will point upward, while the other four will point downward. The triclinic unit cell contains one molecule per unit cell and has the following parameters: a = 9.924 Å, b = 10.564 Å, c = 7.617 Å, α = 97.66°, β = 109.47°, and γ = 92.35°.[71] The tetragonal unit cell measures $a = b$ = 14.93 Å and c = 13.84 Å and contains four molecules.[72] In a triclinic crystal four adjacent ethyl groups will point up or down, causing a C_{2h} symmetry, while in a tetragonal crystal, pairs of ethyl groups will point up or down, resulting in D_4 or D_{2d} symmetry. Because in our STM images the NiOEP molecules are symmetrical and because a strong interaction of the porphyrin ring with the gold substrate exists, it is unlikely for a variation of either crystal structure to occur on a surface. In the tetragonal NiOEP crystal, the main porphyrin ring is also twisted considerably, deviating from the mostly planar structure it has when confined to a surface.[73] The triclinic crystal on the other hand has $\pi-\pi$ interactions between the pyrrole rings and the macrocycle of stacked layers. However, similarly to the triclinic NiTPP crystal, no two porphyrin rings are located in the same plane. This fact combined with the different positioning of the ethyl groups makes the formation of a variation of the NiOEP crystal structure on a substrate improbable. Additionally, the alternating rotated rows we find in the monolayer are not present in any of the NiOEP crystals, indicating an influence of the substrate on the monolayer structure. Our conclusion is that the molecular shape and arrangements in the crystal are too different from the NiOEP monolayer, making any useful deductions about how different interactions influence the structure unlikely.

c.3. Kinked Step Edges Guide Chiral Domains. We continue our discussion of what drives the formation of chiral domains by addressing how the structural equivalence of the racemic packing structures of NiTPP can be broken using kinked steps in the gold surface. As mentioned previously, on large flat terraces of Au(111), NiTPP forms a racemic domain mixture of a square- or parallelogram-shaped unit cell. We have determined that this self-assembly is dominated by intermolecular forces on smooth surfaces. However, the presence of a kinked step changes this situation, and the local structure of the porphyrins is guided by the symmetry of the kink and forms one enantiomeric domain. It seems as though the kinks serve as a nucleation site for chiral domains, forcing the porphyrin array into one of the mirror image structures.[74] Similar behavior was observed in a recent study by Yang et al., where a step edge in a Au(111) surface affected the terrace structure of self-assembled CoTPP domains. In Figure 7, it is shown that an array of NiTPP follows the steps on the Au(111) surface and locally forms domains of only one enantiomer. The kinks on the steps are left-handed kinks and only the left-handed, S′, domain forms. The length of the kinks, the angle between kinks, and the width of the terraces make it possible to elucidate the underlying lattice structure needed to drive this specific local assembly of porphyrin molecules. Along the marked area in Figure 7, the terrace is made up of six NiTPP molecules, and the kink is four molecules long. These distances correspond to approximately 25 gold atoms across the terrace and kinks separated by four gold atoms. A substrate lattice that would lead to the formation of a similar NiTPP array would have the Miller indices (336 316 315). Such a vicinal surface would have (111) terraces that are 25 gold atoms wide, single-atom (110) steps, and (100) kinks.

The local chirality at the kinked steps is able to control the self-assembly of the porphyrin adsorbate on the corresponding gold terraces. The fact that a local kinked step can pattern an area of molecules has tremendous implications. One can imagine the possibilities when the surface chirality is present not as a local defect but extending across the macroscopic surface. This can be realized by using a high Miller index: one handedness of the kinked steps would be present in a large majority across the entire surface. If NiTPP molecules were to be deposited on such a surface, the existence of one of the structural enantiomers should be observed globally, producing a chiral interface. The image shown in Figure 7, which spans two locally kinked steps, demonstrates that this should indeed be possible. A study to extend our findings that kinked steps indeed influence the chirality of the domains is currently underway in our laboratory.

CONCLUSIONS

NiTPP and NiOEP thin films were vapor deposited onto a Au(111) surface and studied using STM imaging and STS spectroscopy. From STM images of the well-ordered porphyrin domains the packing arrangement could be determined, revealing the existence of rotational mirror image domains for both NiTPP and NiOEP. A previously unknown "parallelogram" packing structure was found for NiTPP as well as the expected roughly "square" arrangement. NiOEP formed the expected conformation that has alternate rows which are rotated 15° with respect to each other. Even though both porphyrins are achiral in the gas phase, they form chiral domains on the surface. We conclude that when the porphyrins are assembled on a flat terrace, their chiral packing structure is determined by intermolecular forces that cause the molecules to rotate with respect to each other. Moreover, we demonstrate that it is possible to use a kinked step as a local symmetry-breaking template to lift the structural equivalence of the racemic packing structures of NiTPP that exist on a smooth surface. We are continuing to investigate in detail how intermolecular forces and molecular structure guide the formation of chiral domains of both porphyrin systems and are expanding our effort to include well-defined and intentionally fabricated kinked stepped surfaces to extend these initial findings to macroscopic dimensions.

ACKNOWLEDGMENT

This work was funded by the Office of Basic Energy Sciences, Office of Science, U.S. Department of Energy, Grant DE-SC0002583, and infrastructure support from the NSF-Materials Research Science and Engineering Center at The University of Chicago. Seed funding for this work was provided by the Army Research Office/DTRA. The authors thank Christopher Fleming, Dan Killelea and Miki Nakayama for valuable discussions.

REFERENCES

(1) Scudiero, L.; Hipps, K. *J. Phys. Chem. C* **2007**, *111*, 17516–17520.
(2) Jung, T.; Schlittler, R.; Gimzewski, J. *Nature* **1997**, *386*, 696–698.
(3) Yokoyama, T.; Tomita, Y. *J. Chem. Phys.* **2008**, *129*, 164704 (1−7).
(4) Lei, S.; Wang, J.; Dong, Y.; Wang, C.; Wan, L.; Bai, C. *Surf. Interface Anal.* **2002**, *34*, 767–771.
(5) Wakayama, Y.; Hill, J.; Ariga, K. *Surf. Sci.* **2007**, *601*, 3984–3987.
(6) Fukuzumi, S. *Phys. Chem. Chem. Phys.* **2008**, *10*, 2283–2297.
(7) Suslick, K.; Rakow, N.; Kosal, M.; Chou, J. *J. Porphyrins Phthalocyanines* **2000**, *4*, 407–413.
(8) Friesen, B. A.; Wiggins, B.; McHale, J. L.; Mazur, U.; Hipps, K. W. *J. Am. Chem. Soc.* **2010**, *132*, 8554–8556.
(9) Rakow, N.; Suslick, K. *Nature* **2000**, *406*, 710–713.
(10) Keinan, S.; Therien, M.; Beratan, D.; Yang, W. *J. Phys. Chem. A* **2008**, *112*, 12203–12207.
(11) Senge, M.; Fazekas, M.; Notaras, E.; Blau, W.; Zawadzka, M.; Locos, O.; Mhuircheartaigh, E. *Adv. Mater.* **2007**, *19*, 2737–2774.
(12) Chylarecka, D.; Wäckerlin, C.; Kim, T.; Müller, K.; Nolting, F.; Kleibert, A.; Ballav, N.; Jung, T. *J. Phys. Chem. Lett.* **2010**, *1*, 1408–1413.
(13) Yoshimoto, S.; Tada, A.; Suto, K.; Narita, R.; Itaya, K. *Langmuir* **2003**, *19*, 672–677.
(14) Yoshimoto, S.; Inukai, J.; Tada, A.; Abe, T.; Morimoto, T.; Osuka, A.; Furuta, H.; Itaya, K. *J. Phys. Chem. B* **2004**, *108*, 1948–1954.
(15) Yoshimoto, S.; Tsutsumi, E.; Suto, K.; Honda, Y.; Itaya, K. *Chem. Phys.* **2005**, *319*, 147–158.
(16) Mochida, I.; Suetsugu, K.; Fujitsu, H.; Takeshita, K. *J. Phys. Chem.* **1983**, *87*, 1524–1529.
(17) Visser, J.; Katsonis, N.; Vicario, J.; Feringa, B. L. *Langmuir* **2009**, *25*, 5980–5985.
(18) Pasteur, M. L. *Ann. Chim. Phys.* **1848**, *24*, 442–459.
(19) Rosenberg, R.; Abu Haija, M.; Ryan, P. *Phys. Rev. Lett.* **2008**, *101*, 178301(1−4).
(20) Li, H.; Xu, B.; Evans, D.; Reutt-Robey, J. E. *J. Phys. Chem.* **2007**, *111*, 1202–1206.
(21) Fraile, J. M.; Garcia, J. I.; Herreras, C. I.; Mayoral, J. *Chem. Soc. Rev.* **2009**, *38*, 695–706.
(22) Horvath, J.; Baker, L.; Gellman, A. *J. Phys. Chem. C* **2008**, *112*, 7637–7643.
(23) Yablon, D.; Giancarlo, L.; Flynn, G. *J. Phys. Chem. B* **2000**, *104*, 7627–7635.
(24) Neuber, M.; Schneider, F.; Zubragel, C.; Neumann, M. *J. Phys. Chem.* **1995**, *99*, 9160–9168.
(25) Zhang, J.; Li, B.; Cui, X.; Wang, B.; Yang, J.; Hou, J. G. *J. Am. Chem. Soc.* **2009**, *131*, 5885–5890.
(26) Barrena, E.; Palacios-Lidon, E.; Munuera, C.; Torrelles, X.; Ferrer, S.; Jonas, U.; Salmeron, M.; Ocal, C. *J. Am. Chem. Soc.* **2004**, *126*, 385–395.
(27) Linares, M.; Iavicoli, P.; Psychogyiopoulou, K.; Beljonne, D.; De Feyter, S.; Amabilino, D.; Lazzaroni, R. *Langmuir* **2008**, *24*, 9566–9574.
(28) Berg, A.; Patrick, D. *Angew. Chem., Int. Ed.* **2005**, *44*, 1821–1823.
(29) Mallat, T.; Orglmeister, E.; Baiker, A. *Chem. Rev.* **2007**, *107*, 4863–4890.
(30) Ernst, K. In *Supramolecular Chirality*; Crego-Calama, M., Reinhoudt, D. N., Eds.; Springer-Verlag GmbH: Berlin/Heidelberg, 2006; Vol. 265, pp 209−252.
(31) Mugarza, A.; Lorente, N.; Ordejón, P.; Krull, C.; Stepanow, S.; Bocquet, M. L.; Fraxedas, J. *Phys. Rev. Lett.* **2010**, *105*, 115702-1–4.
(32) Ahmadi, A.; Attard, G.; Feliu, J.; Rhodes, A. *Langmuir* **1999**, *15*, 2420–2424.
(33) Scudiero, L.; Barlow, D.; Mazur, U.; Hipps, K. *J. Am. Chem. Soc.* **2001**, *123*, 4073–4080.
(34) Scudiero, L.; Barlow, D.; Hipps, K. *J. Phys. Chem. B* **2000**, *104*, 11899–11905.
(35) Yoshimoto, S.; Tada, A.; Suto, K.; Yau, S.; Itaya, K. *Langmuir* **2004**, *20*, 3159–3165.
(36) Scudiero, L.; Barlow, D.; Hipps, K. *J. Phys. Chem. B* **2002**, *106*, 996–1003.
(37) Ogunrinde, A.; Hipps, K.; Scudiero, L. *Langmuir* **2006**, *22*, 5697–5701.
(38) Yoshimoto, S.; Tada, A.; Itaya, K. *J. Phys. Chem. B* **2004**, *108*, 5171–5174.
(39) Yoshimoto, S.; Suto, K.; Tada, A.; Kobayashi, N.; Itaya, K. *J. Am. Chem. Soc.* **2004**, *126*, 8020–8027.
(40) Barth, J.; Brune, H.; Ertl, G.; Behm, R. *Phys. Rev. B* **1990**, *42*, 9307–9318.

(41) Woll, C.; Chiang, S.; Wilson, R.; Lippel, P. *Phys. Rev. B* **1989**, *39*, 7988–7991.
(42) Narasimhan, S.; Vanderbilt, D. *Phys. Rev. Lett.* **1992**, *69*, 1564–1567.
(43) Clair, S.; Pons, S.; Fabris, S.; Baroni, S.; Brune, H.; Kern, K.; Barth, J. *J. Phys. Chem. B* **2006**, *110*, 5627–5632.
(44) Suto, K.; Yoshimoto, S.; Itaya, K. *J. Nanosci. Nanotechnol.* **2009**, *9*, 288–294.
(45) Pearl, T.; Sibener, S. *Rev. Sci. Instrum.* **2000**, *71*, 124–127.
(46) Horcas, I.; Fernandez, R.; Gomez-Rodriguez, J.; Colchero, J.; Gomez-Herrero, J.; Baro, A. *Rev. Sci. Instrum.* **2007**, *78*, 013705-1–7.
(47) Comanici, K.; Buchner, F.; Flechtner, K.; Lukasczyk, T.; Gottfried, J.; Steinruck, H.; Marbach, H. *Langmuir* **2008**, *24*, 1897–1901.
(48) Lu, X.; Hipps, K.; Wang, X.; Mazur, U. *J. Am. Chem. Soc.* **1996**, *118*, 7197–7202.
(49) Lu, X.; Hipps, K. *J. Phys. Chem. B* **1997**, *101*, 5391–5396.
(50) Auwarter, W.; Weber-Bargioni, A.; Brink, S.; Riemann, A.; Schiffrin, A.; Ruben, M.; Barth, J. *ChemPhysChem* **2007**, *8*, 250–254.
(51) Auwarter, W.; Weber-Bargioni, A.; Riemann, A.; Schiffrin, A.; Groning, O.; Fasel, R.; Barth, J. *J. Chem. Phys.* **2006**, *124*, 194708-1–6.
(52) Gouterman, M. *J. Mol. Spectrosc.* **1961**, *6*, 138–163.
(53) Kadish, K. M.; Smith, K. M.; Guilard, R. *The Porphyrin Handbook*; Academic Press: San Diego, 2003.
(54) Deng, W.; Hipps, K. *J. Phys. Chem. B* **2003**, *107*, 10736–10740.
(55) Moresco, F.; Meyer, G.; Rieder, K.; Ping, H.; Tang, H.; Joachim, C. *Surf. Sci.* **2002**, *499*, 94–102.
(56) Fleischer, E. B.; Webb, L. E.; Miller, C. K. *J. Am. Chem. Soc.* **1964**, *86*, 2342–2347.
(57) Fleischer, E. B. *J. Am. Chem. Soc.* **1963**, *85*, 1353–1354.
(58) Barlow, D.; Scudiero, L.; Hipps, K. *Langmuir* **2004**, *20*, 4413–4421.
(59) Boeckl, M.; Bramblett, A.; Hauch, K.; Sasaki, T.; Ratner, B.; Rogers, J. *Langmuir* **2000**, *16*, 5644–5653.
(60) Scudiero, L.; Hipps, K.; Barlow, D. *J. Phys. Chem. B* **2003**, *107*, 2903–2909.
(61) Buchner, F.; Flechtner, K.; Bai, Y.; Zillner, E.; Kellner, I.; Steinruck, H.; Marbach, H.; Gottfried, J. *J. Phys. Chem. C* **2008**, *112*, 15458–15465.
(62) Buchner, F.; Schwald, V.; Comanici, K.; Steinruck, H.; Marbach, H. *ChemPhysChem* **2007**, *8*, 241–243.
(63) Rojas, G.; Chen, X.; Cameron, B.; Kim, J.; Kim, J.; Xiao, J.; Dowben, P.; Gao, Y.; Zeng, X.; Choe, W.; Enders, A. *J. Phys. Chem. C* **2010**, *114*, 9408–9415.
(64) Nilsson, D.; Watcharinyanon, S.; Eng, M.; Li, L.; Moons, E.; Johansson, L.; Zharnikov, M.; Shaporenko, A.; Albinsson, B.; Martensson, J. *Langmuir* **2007**, *23*, 6170–6181.
(65) Auwärter, W.; Seufert, K.; Klappenberger, F.; Reichert, J.; Weber-Bargioni, A.; Verdini, A.; Cvetko, D.; Dell'Angela, M.; Floreano, L.; Cossaro, A.; Bavdek, G.; Morgante, A.; Seitsonen, A.; Barth, J. *Phys. Rev. B* **2010**, *81*, 245403-1–14.
(66) Krasnikov, S. A.; Beggan, J. P.; Sergeeva, N. N.; Senge, M. O.; Cafolla, A. A. *Nanotechnology* **2010**, *20*, 135301-1–6.
(67) Kroger, J.; Jensen, H.; Neel, N. *Surf. Sci.* **2007**, *601*, 4180–4184.
(68) Yokoyama, T.; Yokoyama, S.; Kamikado, T.; Mashiko, S. *J. Chem. Phys.* **2001**, *115*, 3814–3818.
(69) Ramoino, L.; von Arx, M.; Schintke, S.; Baratoff, A.; Guntherodt, H.; Jung, T. *Chem. Phys. Lett.* **2006**, *417*, 22–27.
(70) Silvers, S. J.; Tulinsky, A. *J. Am. Chem. Soc.* **1967**, *89*, 3331–3337.
(71) Cullen, D. L.; Meyer, E. F. *J. Am. Chem. Soc.* **1974**, *96*, 2095–2102.
(72) Meyer, E. F. *Acta Crystallogr., Sec. B: Struct. Crystallogr. Cryst. Chem.* **1972**, *28*, 2162–2167.
(73) Czernuszewicz, R. S.; Li, X. Y.; Spiro, T. G. *J. Am. Chem. Soc.* **1989**, *111*, 7024–7031.
(74) Yang, Z. Y.; Durkan, C. *Surf. Sci.* **2010**, *604*, 660–665.